Growth, spectral, optical, and dielectric studies on novel semiorganic NLO single crystal: D-phenylglycine hydrochloride

B. Uma · K. Sakthi Murugesan · R. Jayavel ·
S. Krishnan · B. Milton Boaz

Abstract Good quality novel semiorganic nonlinear optical single crystal of D-phenylglycine hydrochloride has been grown from the aqueous solution by low temperature solution growth method. X-ray diffraction reveals that the crystal crystallises into orthorhombic system with non-centrosymmetric space group $P2_12_12_1$. Experimental parameters are evaluated based on single-crystal XRD and the calculated values of the polarisability were compared with the values of polarisability using Clausius–Mossotti equation. The functional groups present in the grown crystal were confirmed by Fourier transform infrared spectral analysis. The ^1H and ^{13}C FT–NMR has been recorded to elucidate the molecular structure. Ultraviolet–visible-near infra-red absorption studies on this crystal reveal that the minimum absorption region is around 228 nm. The optical band gap of the crystal was found to be 2.9 eV. The scanning electron microscope study has been carried out to determine the surface morphology of the grown crystal. Photoluminescence studies show that the material emits violet fluorescence. Thermal studies bring forth that the crystal is thermally stable up to 255 °C.

Dielectric studies reveal that both the dielectric constant and dielectric loss decrease with the increase in frequency as like the typical semiorganic nonlinear optical crystals such as bisthiourea zinc chloride, bisthiourea cadmium chloride and L-arginine dihydrogen phosphate. Electrical conductivity measurements were carried out and the Arrhenius plot is used to determine the value of activation energy. The Kurtz powder analysis on the crystal confirms the existence of second harmonic generation properties. The SHG efficiency was found to be 1.15 times that of KDP crystal.

1 Introduction

Nonlinear optical phenomenon in materials plays a major role in the emerging photonics and optoelectronic technologies. The design of optoelectronic and photonic devices relies heavily on the development of tailor-made nonlinear optical (NLO) materials with high efficiency. The search for new and efficient NLO materials led to the development of important novel class of materials called semiorganics. These materials have the potentiality of combining high optical nonlinearity and structural diversity or flexibility of organic materials [1] with thermal stability and mechanical strength of inorganic materials [2]. In addition, these class of materials also possess large nonlinearity, high resistance to laser-induced damage and low angular sensitivity [3–5]. Amino acids are interesting organic materials with diverge applications in the field of nonlinear optics. The molecules of amino acids contain a donor carboxylic acid (COOH) group and proton acceptor amino (NH_2) group in them, known as zwitterions which always creates hydrogen bond and are very strong in the molecular interactions. These bonds are widely used in the

B. Uma
Department of Physics, R.M.K. Engineering College,
Kavaraipettai 601206, India

K. Sakthi Murugesan · B. M. Boaz (✉)
PG and Research Department of Physics, Presidency College,
Chennai 600005, India
e-mail: miltonboazcm@yahoo.co.in

R. Jayavel
Crystal Growth Centre, Anna University, Chennai 600025, India

S. Krishnan
Department of Physics, B.S. Abdur Rahman University,
Chennai 600048, India

generation of noncentrosymmetric structures, which is a prerequisite for an effective NLO crystal [6, 7].

Among the organic materials, amino acid constitutes a family, in which glycine is the simplest material possessing high optical and physical properties. Some complexes of amino acid also exhibit ferroelectric properties [8–10]. All the amino acid forms a semiorganic material in combination with inorganic acids. D-phenylglycine is an aromatic mono amino carboxylic amino acid with a nonpolar side group. In this category of amino acids, the side-groups are hydro carbonaceous and thus hydrophobic. It has a benzene ring as a functional group in the side chain. D-phenylglycine is also an important starting material in the production of β-lactams such as semisynthetic cephalosporin's (SSCs) and semisynthetic penicillin's (SSPs) [11]. In view of the above parameters of D-phenylglycine hydrochloride (D-PGHCL), a broad search for the literature report of this material gives only the information about the X-ray crystallographic structure data [12]. As material in bulk form is very much essential for optical devices, in the present investigation attempts were made to grow D-PGHCL in desirable size for technologically important device applications and is obtained successfully by low temperature solution growth technique for the first time. The grown crystal is characterised by single-crystal X-ray diffraction, Fourier transform infrared (FTIR) spectral analysis, FT-NMR analysis, UV–Vis-NIR absorption spectral analysis, SEM analysis, photoluminescence studies, thermogravimetric analysis (TGA), dielectric and NLO studies.

2 Experimental procedure

2.1 Synthesis and crystal growth

The title compound was prepared by dissolving D-Phenyl glycinium and concentrated hydrochloric acid in the molar ratio of 1:1 in deionised water. The solution thus prepared
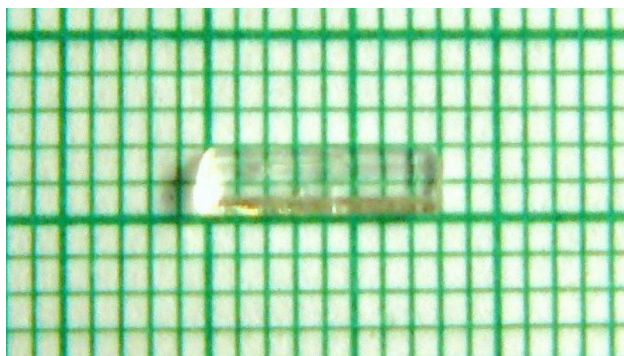
was allowed to evaporate at room temperature to obtain the salt of the crystal in powder form. The synthesised salt was further purified by recrystallisation process. The salt of the crystal according to the solubility data was used in deionised water at saturated temperature to obtain the seed crystals. Good quality seed crystals obtained by homogenous nucleation have been selected and kept inside the mother solution with slight rotation of the solvent. By continuous evaporation of the solvent under rotation, crystals of size $24 \times 4 \times 1$ mm^3 were obtained within a period of 20 days. The photograph of the as grown single crystals is shown in Fig. 1.

2.2 Characterisation

In order to estimate the crystal data of D-PGHCL crystals, single-crystal X-ray diffraction studies have been carried out using an Enraf–Nonius CAD diffractometer with MoKα radiation of wavelength 0.71073A° to determine the cell parameters. The coordination of D-phenylglycine with hydrochloric acid was confirmed by FTIR studies using BRUKKER IFS—66v FTIR spectrometer in the region 4,000–400 cm^{-1} by KBr pellet technique. The ^{1}HNMR and ^{13}C NMR spectrum of the grown crystal has been recorded by Bruker 400 MHz FT-NMR spectrometer in D$_2$O at

Table 1 Crystal data and structure refinement for D-PGHCL crystal

Empirical formula	$C_8H_{10}NO_2$ Cl$^-$
Molecular weight	187.625
Crystal system	Orthorhombic
a	5.4369A°
b	7.2574A°
c	22.771A°
Space group	P2$_1$2$_1$2$_1$
α	90°
β	90°
γ	90°
Volume	898.70A°^{3}
Z	4
Temperature	293 K

Table 2 Experimental parameters of D-PGHCL crystal based on single-crystal XRD

Parameters	Values
Plasma energy	21.59 (eV)
Penn gap energy	1.066 (eV)
Fermi energy	17.72 (eV)
Polarisability	
By Penn analysis	5.317×10^{-23} (cm^3)
By Clausius–Mossotti equation	5.325×10^{-23} (cm^3)

Fig. 1 As grown crystals of D-PGHCL

Fig. 2 FTIR spectrum of D-PGHCL crystal
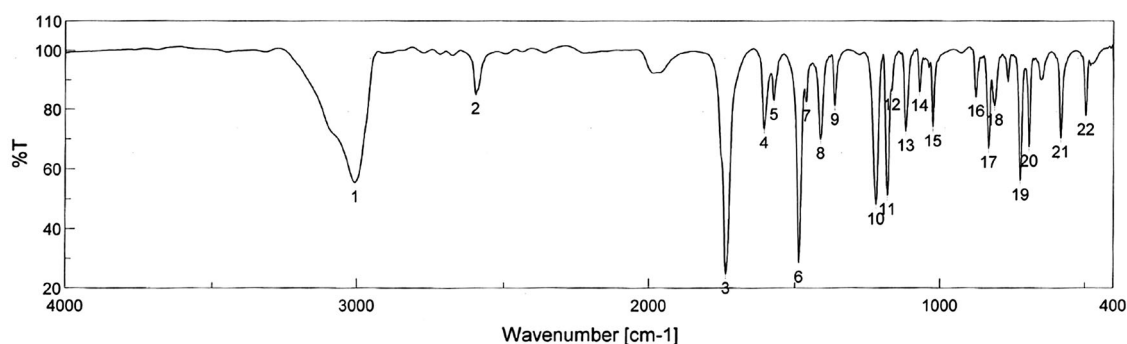
[Result of Peak Picking]

No.	Position	Intensity	No.	Position	Intensity	No.	Position	Intensity
1	3007	55.2762	2	2596	84.8734	3	1737	24.7246
4	1605	73.4175	5	1572	82.967	6	1486	28.4691
7	1461	82.4381	8	1412	69.8593	9	1363	81.2325
10	1221	47.9284	11	1181	51.1014	12	1166	86.2337
13	1118	72.4553	14	1070	85.938	15	1025	73.9932
16	878	84.038	17	833	66.8975	18	813	81.0572
19	724	56.0251	20	693	67.2935	21	583	70.3086
22	497	77.8721						

Table 3 Observed vibrational wave numbers and their assignments for D-PGHCL crystal

Infrared wave numbers in cm^{-1}	Assignments
3,007	φ C–H str (ν_2, ν_{13})
2,596	Overtones and combination bands
1,737	C = O str (resonance interaction)
1,605	φ quad. ring str (ν_{8a})
1,572	φ quad. ring str (ν_{8b})
1,486	φ s.c ring str + CH deformation (ν_{19a})
1,461	φ s.c ring str + CH deformation (ν_{19b})
1,412	Fermi resonance
1,363	Fermi resonance
1,221	φ ring –C str; C–O(H) str
1,181	φ i.p. CH deformation (ν_{9a})
1,166	φ i.p. CH deformation (ν_{15})
1,070	φ i.p. CH deformation (ν_{18b})
878	C–C–N symmetric str
833	C–C str
724	φ o.p. CH deformation (ν_{11})
497	φ o.p. ring deformation (ν_{16b})

quad quadrant, φ phenyl ring, *str* stretching, *i.p.* in plane, *o.p.* out of plane, *s.c.* semicircle

300 K to confirm the molecular structure. The optical transmission spectra of D-PGHCL crystals have been recorded using JASCO UV–Vis-NIR spectrophotometer in the wavelength range of 200 to 900 nm. Surface analysis was carried out through Hitachi-S-3400 N scanning electron microscope. The photoluminescence measurements were made using the Jobin–Yvon-spex make spectrofluorometer (Fluorolog version-3: Model FL3-11) with 450 W high-pressure Xenon lamp as an excitation source. The thermal stability was determined by thermogravimetric analysis and differential thermal analysis using a TGA Q500 V20.10 in an atmosphere of nitrogen at the heating rate of 10 °C/min in the temperature range 30–810 °C. The dielectric studies were carried out using HIOKI 3532 LCR HITESTER in the frequency region from 50 Hz to 5 MHz at various temperatures ranging from 313 to 423 K. The NLO property of the crystal was confirmed by using a Q-switched Nd-YAG laser by employing Kurtz powder second harmonic generation (SHG) test.

3 Results and discussion

3.1 X-ray crystallographic studies

3.1.1 Single-crystal X-ray diffraction studies

Single-crystal X-ray diffraction studies of D-PGHCL single crystals were carried out using an Enraf–Nonius CAD diffractometer with MoKα radiation of wavelength 0.71073A°. Carefully cut crystal of dimension $1 \times 1 \times 2$ mm^3 is used for the analysis. The crystallographic data obtained from single-crystal X-ray data of D-PGHCL crystal are presented in Table 1. From the single-crystal X-ray diffraction analysis, it was observed that the crystal belongs to orthorhombic system with the lattice parameters $a = 5.4369$A°, $b = 7.2574$A°, and $c = 22.771$A° and space group P2$_1$2$_1$2$_1$. The values obtained in the present study are in good agreement with the reported values and thus confirm that the grown crystal is D-PGHCL [12].

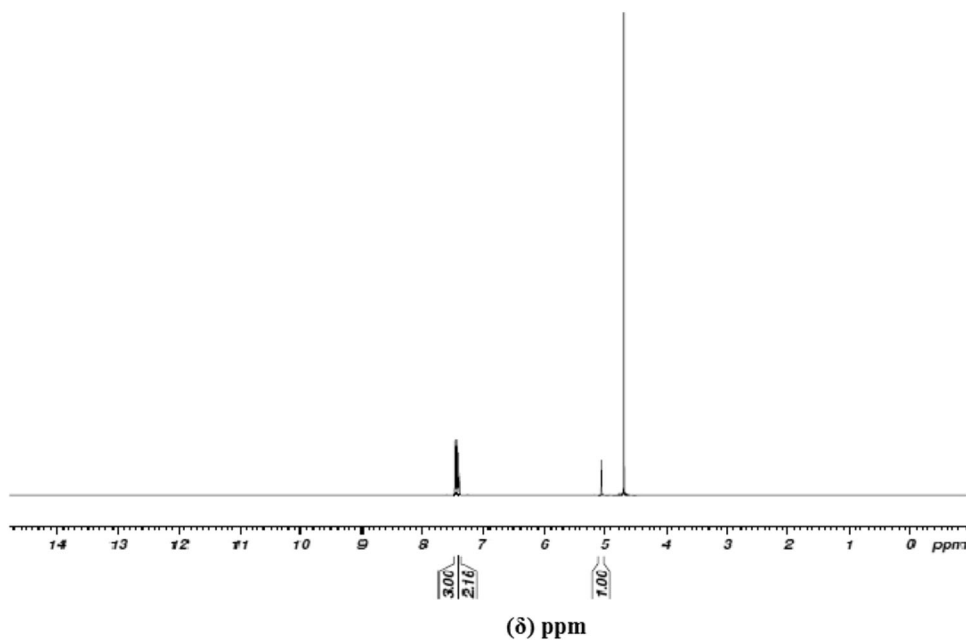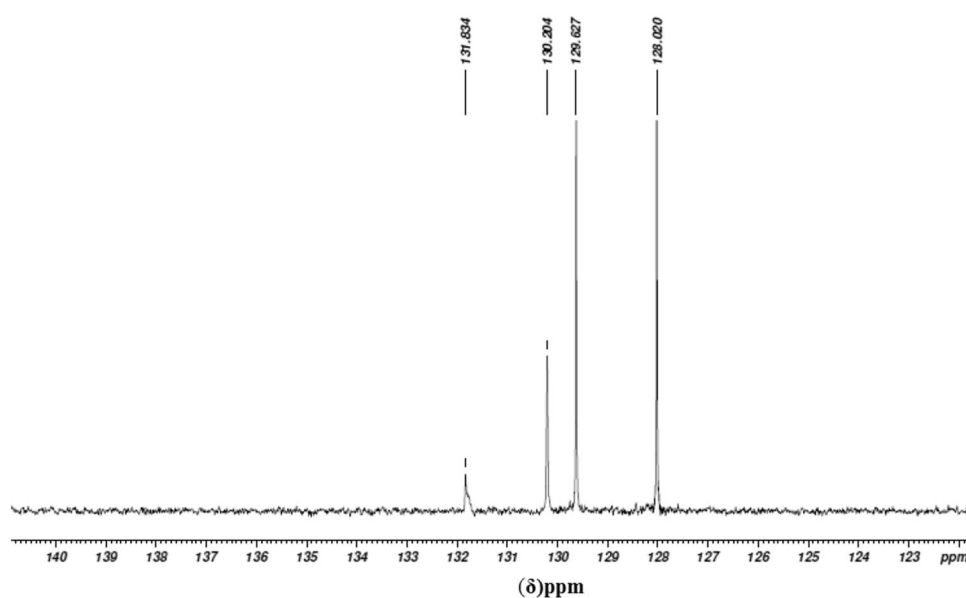**Fig. 3** Proton NMR spectrum
of D-PGHCL crystal

Fig. 4 Carbon NMR spectrum
of D-PGHCL crystal

3.1.2 Experimental parameters based on single-crystal XRD

The valence electron plasma energy, $\hbar\omega_p$, is given by

$$\hbar\omega_p = 28.8\left(\frac{Z_\rho}{M}\right)^{\frac{1}{2}} \tag{1}$$

where $Z = ((4 \times Z_C) + (14 \times Z_H) + (2 \times Z_N) + (6 \times Z_O) + (2 \times Z_{Cl}) + (1 \times Z_{Zn})) = 106$ is the total number of valence electrons, ρ is the density, and M is the molecular weight of the crystal. The Penn gap and the

Fermi energy are explicitly dependent on the $\hbar\omega_p$ [13], which are given by

$$E_P = \frac{\hbar\omega_p}{(\varepsilon_\infty - 1)^{\frac{1}{2}}} \tag{2}$$

$$E_F = 0.2948(\hbar\omega_p)^{\frac{4}{3}} \tag{3}$$

The molecular polarisability, 'α', is obtained by using the relation [20],

$$\alpha = \left|\frac{(\hbar\omega_p)^2 s_O}{(\hbar\omega_p)^2 s_O + 3E_P^2}\right| \times \frac{M}{\rho} \times 0.396 \times 10^{-24}\,\text{cm}^{-1} \tag{4}$$

where S_O is a constant for the material, which is given by

$$S_O = 1 - \left[\frac{E_P}{4E_F}\right] + \frac{1}{3}\left[\frac{E_P}{4E_F}\right]^2 \qquad (5)$$

The value of α so obtained agrees well with that of the Clausius–Mossotti equation, which is given by the relation,

$$\alpha = \frac{3M}{4\pi N_a \rho}\left(\frac{\varepsilon_\infty - 1}{\varepsilon_\infty + 2}\right) \qquad (6)$$

All these experimental parameters evaluated based on single-crystal XRD for the grown crystal are presented in Table 2.

3.2 FTIR analysis

The FTIR spectrum was recorded by the KBr pellet technique in the region 4,000–400 cm^{-1} using a BRUKKER IFS—66v FTIR spectrometer, to confirm the functional groups and qualitative assignments, and is shown in Fig. 2. In the spectrum a broad envelope is found at 3,007 cm^{-1}, which is due to aromatic C–H stretching vibrations in monosubstituted benzenes. The sharp intense peak observed at 1,737 cm^{-1} is assigned to carbonyl stretching vibrations. The quadrant ring stretching components are observed at 1,605 and 1,572 cm^{-1}. The semicircle ring stretching vibration mixes strongly with C–H in-plane bending vibrations and is split into two components (ν_{19a} and ν_{19b}) in substituted benzenes. The ν_{19a} appears at 1,486 cm^{-1} and ν_{19b} appears at 1,461 cm^{-1}. The C–O–(H) stretching vibration is overlapped by phenyl ring carbon stretching vibration. Its corresponding vibration appears in the higher wave number region 1,221 cm^{-1}. The phenyl ring in-plane C–H deformation mode is assigned to 1,181 and 1,166 cm^{-1}. There is a fine structure between 1,070 and 878 cm^{-1}, which illustrates C–C–N asymmetric stretching. A peak at 833 cm^{-1} is due to C–C stretching. The out of plane C–H deformation mode (ν_{11}) appears as a high intensity band around 724 cm^{-1} is due to the large change in dipole moment caused by out of plane movement of five adjacent

hydrogen atoms in the monosubstituted benzene ring. In the monosubstituted benzenes, the out of plane quadrant deformation mode (ν_{16b}) appears as a strong band at 497 cm^{-1}. The frequency assignment of the crystal is presented in Table 3.

3.3 NMR analysis

3.3.1 ^1H NMR analysis

The nuclear magnetic resonance (NMR) spectroscopy is a versatile technique employed in the identification of organic compounds [14]. The ^{1}HNMR spectrum recorded for D-PGHCL crystal was shown in the Fig. 3. The spectrum is due to the presence of protons in the different chemical environments of the given compound. The peak observed at $\delta = 7.38$–7.42 ppm (m, J = 2.16 Hz, 6H) shows multiplet, which is due to aromatic ring. The peak at $\delta = 7.432$–7.47 ppm (m, J = 3 Hz, CH proton) has a triplet and is due to the interaction of CH proton, whereas at $\delta = 5.0$–5.1 ppm (d, J = 1.00 Hz, 2H) gives doublet due to the existence of NH$_2$ group. The occurence of multiple splitting confirms the presence of amine group in the molecular structure [15–17].

3.3.1.1 ^{13}C NMR analysis

From the ^{13}CNMR spectrum shown in Fig. 4, the signal at 56.812 ppm is due to aliphatic carbon carrying NH$_3^+$ ions. The presence of COOH carbon is confirmed by the peak exists at 171.183 ppm. The carbon atom in the aromatic ring gives peaks at 128.020–130.204 ppm. The peak observed at 131.834 ppm may be due to the salt structure. As no other prominent peaks are observed, it is confirmed that the compound has been successfully synthesised as a pure material [18].

3.4 Optical characterisation

3.4.1 Optical absorption studies

The optical absorption spectrum of grown crystal was recorded using JASCO UV–Vis–NIR spectrophotometer in the wavelength range of to 900 nm and is shown in Fig. 5.
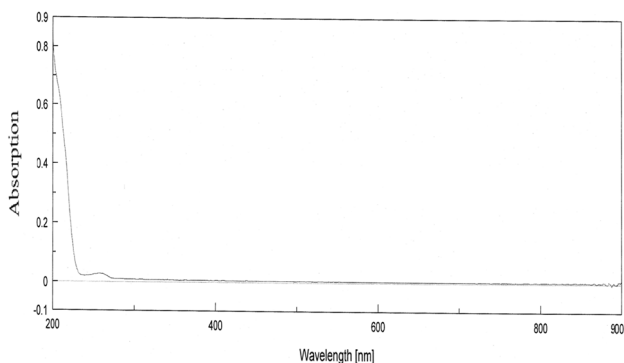
Table 4 Comparison of lower cutoff in the UV spectrum of D-PGHCL with other NLO materials

Compound	Lower UV cutoff wavelength in nm
D-PGHCL	228
L-valine hydrochloride	295
Bis glycine hydrochloride	300
Glycine zinc chloride	240
Glycine zinc sulphate	300
Glycine oxalate	305

Fig. 5 UV spectrum of D-PGHCL crystal
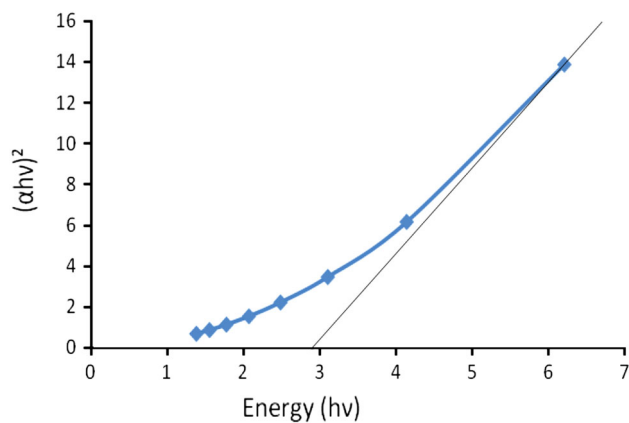
Fig. 6 Band gap of D-PGHCL crystal

Fig. 8 Luminescence spectrum of D-PGHCL crystal

$$\alpha = \frac{1}{d}\log\frac{1}{T} \tag{7}$$

where 'T' is the transmittance and 'd' is the thickness of the crystal.

Owing to the direct band gap, the crystal under study has an absorption coefficient (α) obeying the following relation for high photon energies ($h\nu$)

$$\alpha = \frac{A(h\nu - E_g)^{1/2}}{h\nu} \tag{8}$$

where E_g is the optical band gap of the crystal and A is a constant. The plot of variation of $(\alpha h\nu)^2$ versus ($h\nu$) is shown in Fig. 6. E_g is evaluated by the extrapolation of the linear part [20]. The band gap was found to be 2.9 eV. The colourless nature of the crystal shows its high transmission in the entire UV–VIS—NIR region and the obtained values are in good agreement with the reported values [21].

Fig. 7 SEM analysis of D-PGHCL crystal

Carefull examination of the spectrum reveals that the lower cutoff wavelength is around 228 nm. It is also observed that the crystal is transparent in the ultraviolet, visible, and near infrared regions. The very less absorption of the crystal is due to the delocalisation of electronic cloud available for charge transfer and molecular hyperpolarisation. The less absorption in ultraviolet and visible regions is the most desirable property of the materials possessing NLO activity and also indicates good quality of the crystal for optical applications [19]. The lower cutoff wavelength in the UV spectrum of the grown crystal was compared with other solution grown NLO crystals and the values are presented in Table 4.

3.4.2 Determination of optical band gap

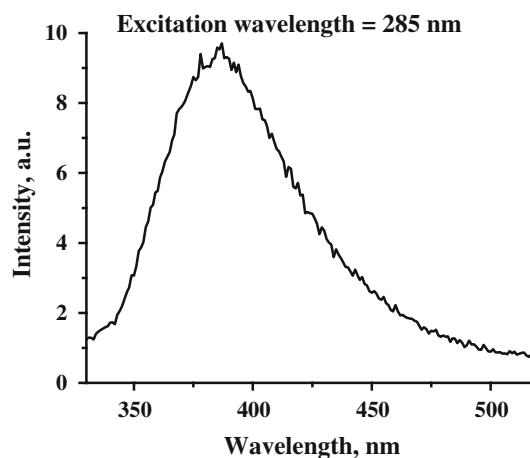The optical absorption coefficient (α) was calculated from the transmittance using the following relation,

3.4.3 SEM analysis

Surface analysis of D-PGHCL was carried out using Hitachi-S-3400 N scanning electron microscope and the SEM micrograph obtained was shown in Fig. 7. Gold carbon coating is given before subjecting the crystal surface to electron beam. The maximum magnification possible in the equipment is 3,00,000 times with a resolution of 10 nm. From the SEM image, it is clear that the surface of the grown crystal appears smooth though it has pots and microcrystal on the surface. Overall, the surface is very smooth with the appearance of few inclusions formed on the crystal during growth and they are influenced by the growth conditions. The grain boundaries are clearly seen, which shows the perfect growth of the crystal.

Fig. 9 TGA/DTA analysis of D-PGHCL crystal
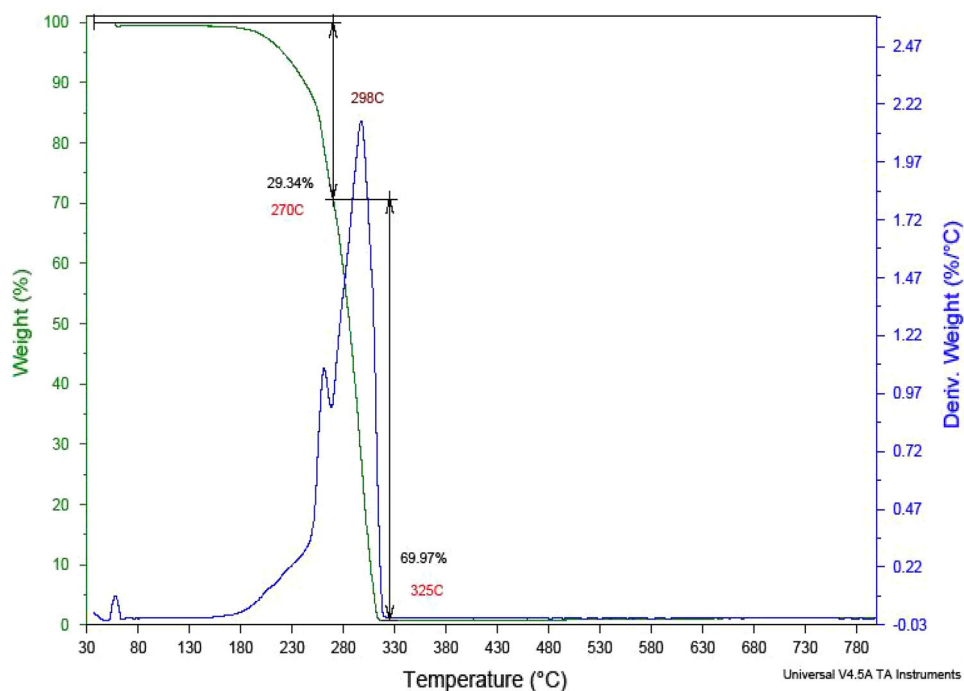
3.4.4 Photoluminescence studies

Photoluminescence is a contactless, nondestructive method of probing the electronic structure of materials [22]. The sample was excited at 285 nm and the emission spectrum was measured in the range of 300–550 nm. From the recorded photoluminescence spectrum shown in Fig. 8, it was observed that the material exhibits a high intense emission peak at 385 nm. Hence, the photoluminescence analysis concludes that D-PGHCL crystal exhibits violet fluorescence. The maximum intensity which appears at 385 nm is attributed to $n - \pi^*$ transition of carbonyl group [23].

3.5 Thermal analysis

Thermogravimetric (TG) analysis for the D-PGHCL was carried out by using the TGA Q500 V20.10 in an atmosphere of nitrogen at the heating rate of 10 °C/min in the temperature range 30–810 °C and is shown in Fig. 9. The TGA analysis reveals that the D-PGHCL has a weight loss of 69.67 % at 325 °C and 29.34 % at 270 °C. The nature of weight loss indicates the decomposition point of the material [24]. The TGA thermogram also brings forth that the crystal has a good thermal stability up to 255 °C. In the DTA spectrum, an irreversible exothermic peak was observed around 298 °C, which confirms the thermal stability of the crystal. From the thermal study, overall it is concluded that the crystal can retain its texture up to 255 °C.
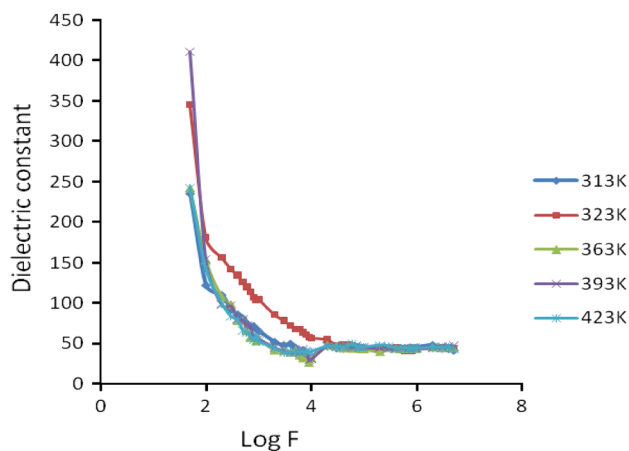

Fig. 10 Variation of dielectric constant with frequency in D-PGHCL crystal

3.6 Dielectric measurements

3.6.1 Dielectric constant and dielectric loss measurements

The dielectric constant and dielectric loss measurements were performed for the grown crystal D-PGHCL of dimension 4.39 × 3.22 × 0.48 mm using the HIOKI 3532 LCR HITESTER in the frequency region from 50 Hz to 5 MHz at various temperatures ranging from 313 to 423 K. The presence of the dielectric between the capacitor plates increases capacitance of the capacitor. The dielectric constant was calculated using the relation,
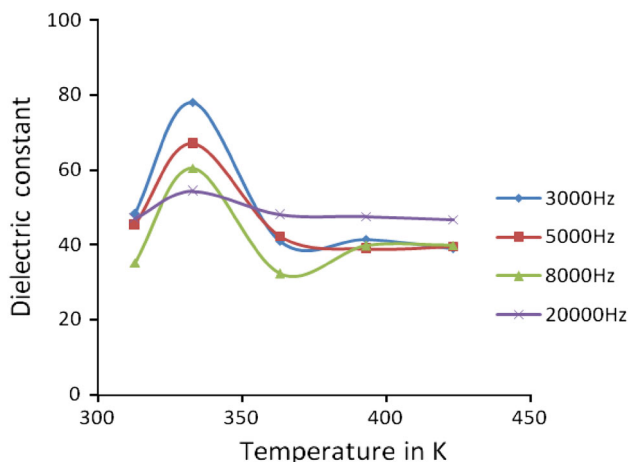
Fig. 11 Variation of dielectric constant with the temperature in D-PGHCL crystal
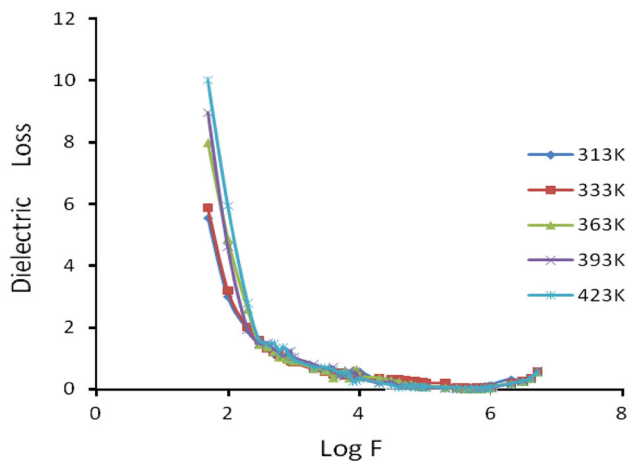

Fig. 12 Variation of dielectric loss with frequency in D-PGHCL crystal

$$\varepsilon = \frac{Cd}{A\varepsilon_O} \qquad (9)$$

where C is the capacitance, d is the thickness of the crystal, A is the area of cross section of the crystal, and ε_O is the permittivity of free space.

The variation of the dielectric constant with the frequency is shown in Fig. 10. The high value of the dielectric constant at low frequencies may be due to the presence of all the four polarisations, namely electronic, ionic, orientation, and space charge polarisations, and the low value at higher frequencies may be due to the loss of significance of these polarisations gradually [25]. The variation of dielectric constant as a function of temperature for varying frequencies is shown in Fig. 11. The profile infer that the crystal behaves as ferroelectric before 323 K and becomes para electric above 323 K, at varying frequencies, which proves the ferroelectric nature of the crystal. The variation
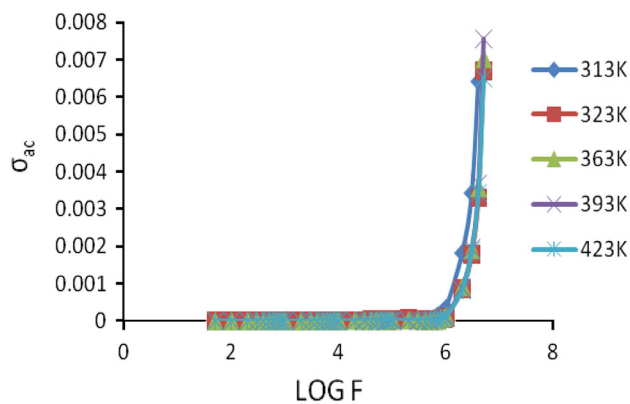

Fig. 13 Variation of AC conductivity with LOG F in D-PGHCL crystal

of dielectric loss with frequency is shown in Fig. 12. The characteristics of low dielectric loss with high frequency for the crystal suggest that it possesses enhanced optical quality with lesser defects and this parameter is important for nonlinear optical applications [26–28].

3.6.2 Electrical conductivity studies

The electrical conductivity in crystals gives an insight into the material properties with respect to transport of ions and electrons. It also gives information regarding relaxation time, mobility and temperature dependence of these properties. The alternating current (AC) conductivity σ_{ac} is calculated using the relation [29],

$$\sigma_{ac} = 2\pi f \varepsilon_o \varepsilon' \tan\delta \qquad (10)$$

where $\tan\delta$ is the dielectric loss measured directly from the impedance analyser and f is the frequency of the applied ac field (Hz). The variation of ac conductivity σ_{ac} with $\log f$ is depicted in Fig. 13.

It was observed that the crystal has very low conductivity in the low-frequency region up to the frequency 50 Hz to 40 kHz for all temperatures. Thereafter, the ac conductivity was found to be increasing feebly up to 4 MHz. However, sharply at 4 MHz, the conductivity increases abruptly for all the measured temperatures, which indicates the dielectric breakdown frequency of this material.

The DC electrical conductivity of the crystal at room temperature is evaluated using the relation,

$$\sigma_{dc} = \frac{d}{AR_{dc}} \qquad (11)$$

where R_{dc} is the total electrical resistance of the sample. The value of R_{dc} is evaluated from the Cole–Cole plots shown in Fig. 14, plotted between $Z' = Z\cos\theta$ (real part of impedance) and $Z'' = Z\sin\theta$ (imaginary part of impedance). From these plots, the bulk resistance (R_{dc}) measured
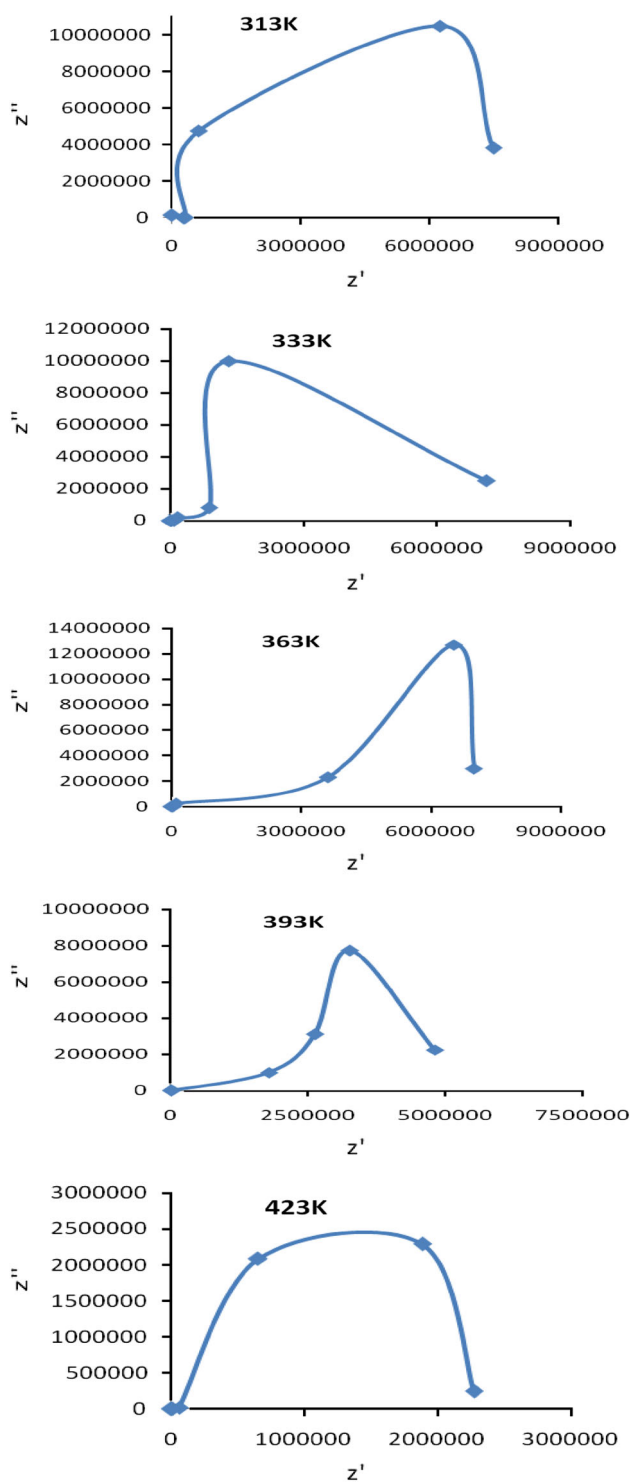
Fig. 14 Cole–Cole plots of D-PGHCL crystal

Table 5 DC conductivity at various temperatures for D-PGHCL crystal

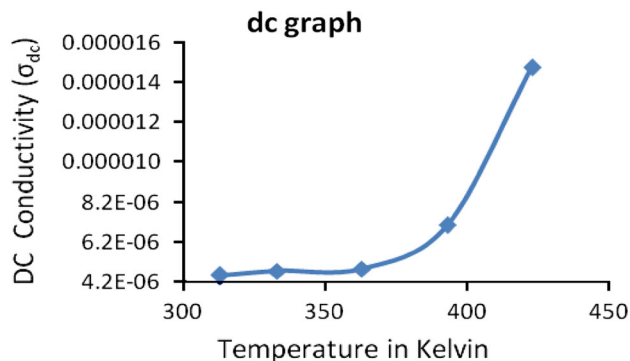| DC conductivity (in mho m^{-1})	Temperatures (in Kelvin)
4.5388×10^{-6}	313
4.7599×10^{-6}	333
4.8531×10^{-6}	363
7.0535×10^{-6}	393
1.4958×10^{-5}	423

Fig. 15 DC conductivity versus temperature of D-PGHCL crystal

conductivity values calculated using the Eq. (11) for various temperatures are presented in Table 5. The variation of DC conductivity versus temperature was shown in Fig. 15. The graph explains the increase in the conductivity with the increase in the temperature due to the increase in mobility and release of ions at elevated temperatures.

The activation energy of the crystal is also calculated from the Arrhenius plot using the relation,

$$\sigma = \sigma_0 \exp\left(-\frac{E_a}{kT}\right) \tag{12}$$

where σ is the conductivity at temperature T, E_a the activation energy for the electrical process and k is the Boltzmann constant. The activation energy was obtained from the plot between $Log\sigma T$ (Ω^{-1} cm^{-1}) and $1{,}000/T$ (K^{-1}) depicted in Fig. 16. The activation energy calculated from the slope of the curve was found to be $E_a = 0.079$ eV.

3.7 NLO test

The SHG property of the grown crystal was studied using a Q-switched Nd-YAG laser by employing Kurtz powder test. The fundamental beam of an Nd-YAG laser with 1064 nm wavelength, pulse duration of 35 ps, and 10 Hz repetition rate is focused on to the powdered sample. The SHG signal at 532 nm is recorded on the sample using a photomultiplier tube and boxcar averager. The emission of
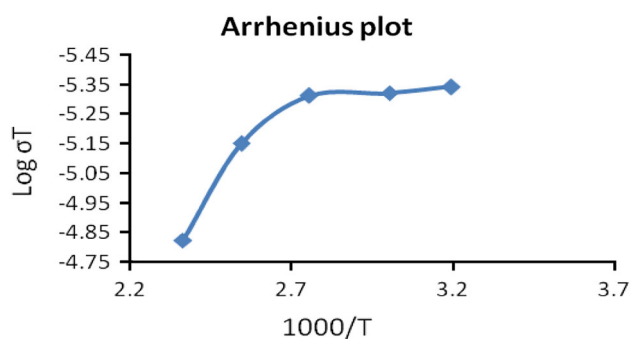
was found to be decrease with increasing temperatures, resulting in the enhancement of electrical conductivity at higher temperatures. The low value of electrical conductivity of GGC crystal is due to the decrease in mobility of the charge carriers by ion size, which brings prominant changes in the electronic band structure. The DC

Fig. 16 Arrhenius plot of D-PGHCL crystal

green light confirms the presence of second order NLO activity in the crystal. The output of SHG signal with the energy of 133 mV confirms the nonlinear behaviour of the crystal and was found to be 1.15 times that of KDP (116 mV for the same input energy) crystal.

4 Conclusion

Single crystals of D-PGHCL were grown by the low temperature solution growth method. The grown crystal was confirmed by single-crystal X-ray diffraction and FTIR analysis. The optical studies reveal that the crystal has very low absorption in the entire visible and infrared region with the lower cutoff wavelength of around 228 nm. FT-NMR spectrum confirms the structure of the compound. Luminescence studies show that D-PGHCL crystal exhibits violet fluorescence. Perfection of the grown crystal and photoluminescence property shows that the grown crystal is suitable for photonic device and laser-related applications. TGA-DTA analysis reveals that D-PGHCL is stable up to 255 °C. The low values of dielectric constant and dielectric loss of the crystal indicate that this material is an excellent candidate for high speed electro-optic modulations. The variation of dielectric constant with temperature at various frequencies proves its ferroelectric behaviour. Further, ferroelectric characterisation is in progress. The variation of the electrical conductivity with the temperatures was analysed using the Cole–Cole plots. The activation energy of the crystal was estimated as $E_a = 0.079$ eV from the Arrhenius plot. The Kurtz SHG test confirms that the grown crystal has SHG efficiency and the measured output SHG power is found to be 1.15 times higher than the standard NLO crystal KDP.

References

1. D.S. Chemla, J. Zyss (eds.), Volumes 1&2. (Academic Press, New York, 1987)
2. P.V. Dhanaraj, N.P. Rajesh, J. Phys. B. **405**, 4105–4110 (2010)
3. G. Xing, M. Jiang, Z. Sao, D. Xu, Chin. J. Lasers **14**, 302 (1987)
4. N. Zhang, M. Jiang, D. Yuan, D. Xu, X. Tao, Chin. J. Phys. Lett. **6**, 280 (1989)
5. H.O. Marcy, L.F. Warren, M.S. Webb, C.A. Ebbers, S.P. Velsko, G.C. Kennedy, G.L. Catella, J. Appl. Opt. **31**, 5051 (1992)
6. G.M. Frankenbach, M.C. Etter, J. Chem. Mater **4**, 272 (1992)
7. R. Hanumantharao, S. Kalainathan, Spectrochimica Acta Part A, **86**, 80–84 (2012)
8. R. Pepinsky, Y. Okaya, D.P. Eastman, T. Mitsui, J. Phys. Rev. **107**, 1538 (1957)
9. R. Pepinsky, K. Vedam, Y. Okaya, J. Phys. Rev. **110**, 1309 (1958)
10. A. Deepthy, H.L. Bhat, J. Cryst. Growth **226**, 287 (2001)
11. S. Ramaswamy, R.K. Rajaram, V. Ramakrishnan, J. Raman Spectrosc. **33**, 689–698 (2002)
12. S. Ravichandran, J.K. Datragupta, C. Chakrabarti, Acta Cryst. **C54**, 499–501 (1998)
13. N.M. Ravindra, R.P. Bharadwaj, K. Sunil Kumar, V.K. Srivastava, J. Infrared Phys. **21**, 369 (1981)
14. J. Ramajothi, S. Dhanuskodi, J. Cryst. Growth **289**, 217–228 (2006)
15. P.Y. Bruice, *Organic Chemistry*, 3rd edn. (Pearson Education, Singapore, 2002)
16. R. Swislocka, Spectrochimica Acta Part A, **100**, 21–30 (2013)
17. X.-H. Li, X.-Z. Zhang, Spectrochimica Acta Part A, **105**, 280–287 (2013)
18. G. Swiderski, M. Kalinowska, R. Swislocka, S. Wojtulewki, W. Lewandowski, Spectrochimica Acta Part A, **100**, 41–50 (2013)
19. R. Uthrakumar, C. Vesta, M. Jose, K. Sugandhi, S. Krishnan, S. Jerome Das, Physica b. **405**, 3371–3375 (2010)
20. A.K. Chawla, D. Kaur, R. Chandra, Optical Mater. **29**, 995–998 (2007)
21. B. Narayana Moolya, S.M. Darmaprakash, J. Crys. Growth **293**, 86–92 (2006)
22. N. Vijayan, G. Bhagavannarayana, K.K. Maurya, S.N. Sharma, Optik **123**, 604–608 (2012)
23. C. Laurent, F. Massines, C. Mayoux, D.M. Ryder, C. Olliff, IEEE Conference, 93–96 (1995)
24. U. Charoen-In, P. Ramasamy, P. Manyum, J. Cryst. Growth **312**, 2369–2375 (2010)
25. C.P. Smyth, *Dielectric Behavior and Structure* (McGraw-Hill, New York, 1965) p. 132
26. C. Balarew, R. Duhlew, J. Solid State Chem. **55**, 1 (1984)
27. P. Pandi, G. Peramaiyan, S. Sudhakar, G. Chakkaravarthi, R. Mohan kumar, G. Bhagavan narayana, R. Jayavel, Spectrochimica Acta Part A, **98**, 7–13 (2012)
28. R. Hanumantharao, S. Kalainathan, G. Bhagavan narayana, U. Madhusoodanan, Spectrochimica Acta Part A, **103**, 388–399 (2013)
29. B. Lal, K.K. Barnzai, P.N. Kotru, B.M. Wanklyn, Mater. Chem. Phys. **85**, 353–365 (2004)